UCRL- 91490 Rev. 1
PREPRINT

THE MOTION OF THIN METAL WALLS AND THE EQUATION OF STATE OF DETONATION PRODUCTS

E. Lee
D. Breithaupt
C. McMillan
N. Parker
J. Kury
C. Tarver
W. Quirk
J. Walton

Prepared for submittal to the 8th Symposium
on Detonation, Albuquerque, NM
July 15-19, 1985

November 21, 1985

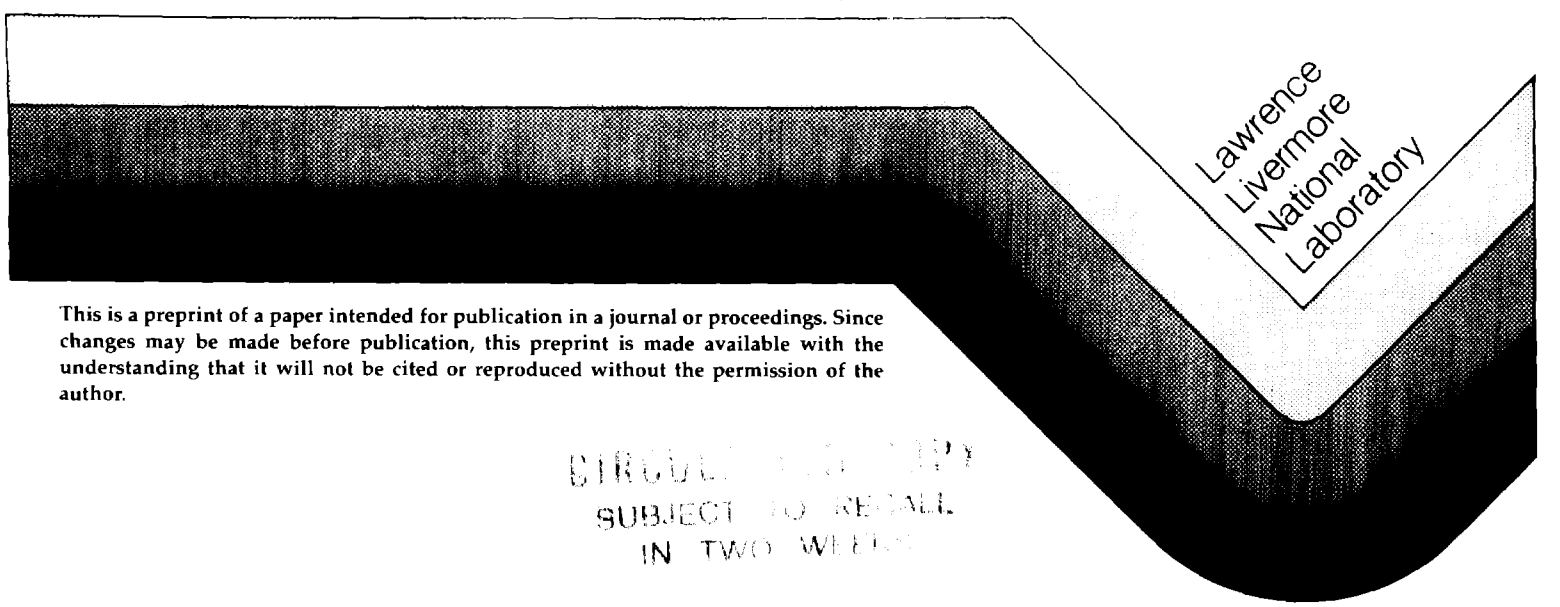

THE MOTION OF THIN METAL WALLS AND THE EQUATION OF STATE OF DETONATION PRODUCTS*

E. Lee, D. Breithaupt, C. McMillan, N. Parker, J. Kury,
C. Tarver, W. Quirk, and J. Walton
Lawrence Livermore National Laboratory
University of California
Livermore, CA 94550

This paper reports dynamic high resolution measurements made using metal cylinders and flat plates accelerated by explosives to determine detonation product behavior. By using both thin walled cylinders and plates and by utilizing both streak camera and Fabry-Perot velocimeter techniques, resolution and accuracy greater than previously attained was achieved. As an example, results for LX-14, an explosive containing 95% HMX and 5% polyurethane, are presented and compared to results of hydrodynamic calculations carried out with an accuracy equivalent to the experimental resolution. Calculations show that cylinder test measurements sample the detonation product equation of state (EOS) at expansion ratios $V/V_o > 1$. Thin flat plates aligned in the plane of the detonation front provide detailed information on the higher compression states ($V_{CJ} < V/V_o < 1.3$). The results of this study confirm earlier work with respect to the pressure derivatives. The results require that $(\partial \ln P/\partial \ln V)_S$ first increase as the products expand from the C-J state.

INTRODUCTION

Accurate experimental measurements of detonation product equations of state are needed both for precision applications and for basic studies of product behavior. The pressure range of interest is from 0.1 GPa to over 40 GPa and a temperature range from 1000°K and 4000°K. Because of the combination of high temperature and very high pressure, static pressure measurement techniques cannot be used to measure the equation of state for the mixture of gases and solids produced in a detonation. For this reason dynamic measurements have traditionally been used to evaluate detonation product equations of state.

Some of the earliest work[1] utilized the dependence of detonation velocity on loading density. A technique using witness materials[2,3] to determine pressure at the detonation front from shock impedance relationships is still used extensively. We have previously shown[4] that the velocity history of an explosively expanded copper cylinder can be used to develop a detonation product equation of state. The earlier work was limited by the geometry of the test and the resolution of our rotating mirror camera (RMC) measurement techniques. In particular, there were large uncertainties in the pressure regime above 10 GPa.

In order to obtain more precise data at high pressures, modifications have been made in the cylinder test and a flat plate test has been developed. Much greater accuracy and resolution can now be obtained by using Fabry-Perot velocimeters.[5] We have also made modifications to the RMC slit measurement technique and have compared the two techniques.

This paper describes the experimental techniques and presents results obtained for the plastic bonded explosive LX-14. The data are used to refine the LX-14 detonation product equation of state previously determined from the cylinder test. Modern computer capacity and speed permits calculations with resolution comparable to the experimental measurements. Detailed material models can be implemented to study both the explosive and the witness materials. We will use hydrodynamic calculations to show the sensitivity of the results to changes in the equation of state.

EXPERIMENTAL

LX-14

The explosive used in this investigation was LX-14 containing 95.5% HMX and 4.5% estane 5702-F1. This plastic bonded explosive contains some HMX crystals that are 400 μ or larger in diameter. The cylinder experiments and most of the flat plate experiments were performed with this material pressed to 98.3 ± 0.3 percent of theoretical maximum density.

*Work performed under the auspices of the U.S. Department of Energy by the Lawrence Livermore National Laboratory under contract No. W-7405-ENG-48.

In order to explore particle size effects, a special fine grained version of LX-14 was prepared containing HMX crystals with diameters < 40 μ. This formulation was used in some of the flat plate experiments.

Cylinder Experiments

The configuration for the cylinder test has been modified for the work described here as shown in Fig. 1. Important features which differ from earlier work[4] are that a large plane wave booster is used to provide an initiation source which is as flat and as nearly normal to the tube axis as possible. The pin rings, one near each end of the cylinder, are used to determine detonation velocity but are also indexed so as to measure any tilt in the detonation wave.

Most of the previous cylinder tests were done with 1.000" inside diameter copper tubes having 0.100" thick walls. We now use 2.000" inside diameter tubes with 0.100" thick walls. This geometry provides twice the time resolution in monitoring the pressure change in the detonation products.

In our earlier work two Model 75 streak cameras were used to measure the rate of cylinder expansion by observing the shadow of the back-lighted cylinder moving across the camera slit. A Model 132 streak camera is now also used to monitor cylinder expansion. This rotating mirror camera is run over three times as fast as the Model 75 cameras to better resolve the initial wall motion.

The principal modification is the addition of Fabry-Perot velocimeters to measure cylinder wall velocities directly. The two velocimeters are positioned to look at opposite sides of the cylinder at close to the same area monitored by the streak cameras. Comparison of results obtained by these independent techniques provide assurance of the precision and accuracy of the measurements.

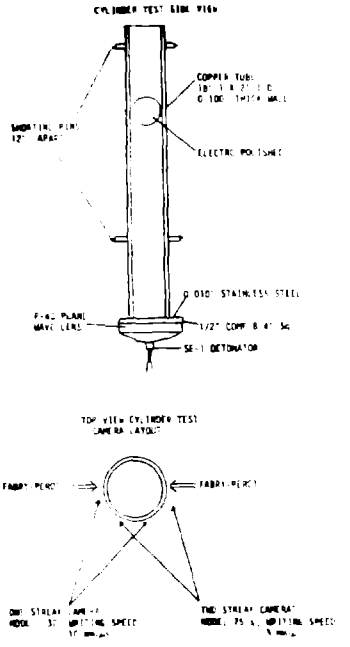

Fig. 1 Cylinder experiment.

Flat Plate Experiments

The geometries used in the flat plate experiments are shown in Figs. 2a and 2b. An electric gun[6] was used to initiate all except the 100-mm long LX-14 charges. These charges were initiated with a P-040 lens and 0.50" of Comp. B. Both initiation systems produce flat wave profiles and prompt initiation of LX-14.

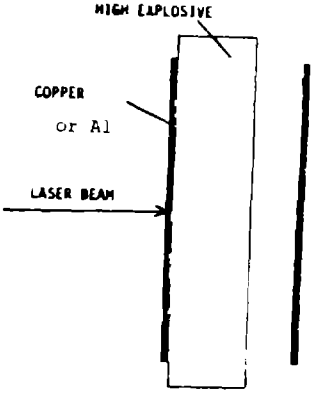

Fig. 2a Flat plate experiment - electric gun initiation.

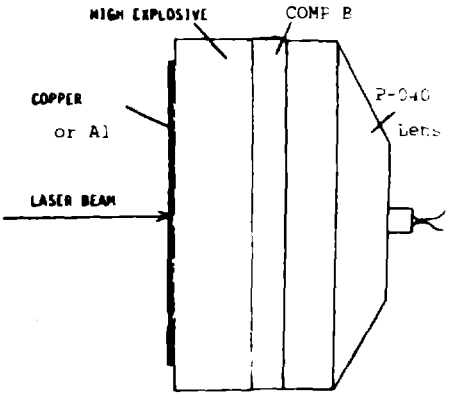

Fig. 2b Flat plate experiment - plane wave lens initiation.

CALCULATIONAL METHODS

The hydrodynamic analysis of the cylinder experiments was done using the 2D Lagrangian code HEMP[7] and the 1D Lagrangian code KOVEC[8] was used for the flat plate experiments. The speed and memory size of the Cray computers now allow fine enough zoning so that calculational resolution using these codes are comparable to the experimental resolution. A series of HEMP calculations were run to determine the effect of varying the zoning in cylinder test calculations. Resolution to that of the experiment was obtained with 0.02-cm axial and 0.011-cm radial zones in the copper and 0.04-cm axial and 0.053-cm radial zones in the explosive. This zoning was used for the cylinder test 2D calculations presented in this report.

The JWL equation of state[4] for the detonation products was used in the hydrodynamic calculations (Eq. 1).

$$P = A\left(1 - \frac{\omega}{R_1 V}\right)e^{-R_1 V} + B\left(1 - \frac{\omega}{R_2 V}\right)e^{-R_2 V} + \frac{\omega E}{V} \qquad (1)$$

where V = relative volume. This form is very flexible and permits analytic calculation of the pressure and energy. The important results are those derived from comparisons of experiments and calculations. These comparisons reveal the precision to which one can determine the equation of state of the detonation products. To this end the results are independent of the form of the EOS.

The Gruneisen equation of state was used for copper and aluminum. The coefficients used in Eqs. 2 and 3 are presented in Table 1.

$$U_s = C + S_1 U_p + S_2 U_p^2 + S_3 U_p^3 \qquad (2)$$

$$P = \frac{P_0 C^2 \mu\left[1 + (1 - \frac{\gamma_0}{2})\mu - \frac{a}{2}\mu^2\right]}{\left[1 - (S_1 - 1)\mu - S_2\left(\frac{\mu^2}{\mu + 1}\right) - S_3\left(\frac{\mu^2}{(\mu + 1)^2}\right)\right]^2} + (\gamma_0 + a\mu)e \qquad (3)$$

where $\mu = \frac{\rho}{\rho_0} - 1$.

TABLE 1
Gruneisen Equation of State Coefficients

	ρ_0	C	S_1	S_2	S_3	γ_0	a
Copper	8.93	0.394	1.489	0.0	0.0	2.02	0.47
Aluminum	2.703	0.524	1.40	0.0	0.0	1.97	0.48

CYLINDER TESTS

Experimental Results

The streak camera records obtained from the cylinder test are read on a precision comparator. A computer program converts film coordinates into actual radius (R) at the slit and time, fits the data and calculates the wall arrival time at specified values of $R - R_0$. The results obtained for LX-14 at a density of 1.830 gm/cc are presented in Table 2.

The Fabry-Perot velocimeter system consists of a cylindrical lens, a Fabry-Perot interferometer, a spherical lens, and an electronic streak camera. It works on the principle of recording the position vs. time of Fabry-Perot fringes produced by the Doppler-shifting reflected light from the cylinder wall. The fringes are produced by virtue of the fact that the Fabry-Perot interferometer will pass light at only select discrete angles determined by the Fabry-Perot mirror spacing and the light wavelength. Light reflected from a target moving at constant velocity, though Doppler shifted, will give a static pattern. Accelerating the target will cause the reflected beam to be Doppler shifted to higher frequencies and result in an expanding pattern. The change in pattern is related to the change in velocity by the expression:

$$V(t) = \frac{\lambda c}{4L}\left[\frac{D_f^2(t) - D_{f_0}^2}{D_{f_{20}}^2 - D_{f_0}^2} + m\right] \qquad (4)$$

where λ = the initial beam wavelength, c = the velocity of light, L = the separation of the Fabry-Perot mirrors, D_{10} and D_{20} are the spacing of adjacent pairs of lines in the static pattern, and $D_1(t)$ is the spacing of the expanded pattern. Should the velocity excursion exceed the range between fringes, m is the number of fringes traversed.

TABLE 2
Radius-Time History of Copper Cylinder Expanded by LX-14

50.8-mm Diameter LX-14
2.725-mm Thick Copper Wall

$R-R_o$ (mm)	t (μsec)
0	0
1.0	1.01
2.0	1.78
3.0	2.42
4.0	3.02
5.0	3.56
6.0	4.10
7.0	4.60
8.0	5.10
9.0	5.58
10.0	6.07
12.0	7.02
14.0	7.94
16.0	8.85
18.0	9.73
20.0	10.62
25.0	12.80
30.0	14.92
35.0	17.01

In order to compare the cylinder test data from the Fabry-Perot velocimeter with the radius/time data taken from the rotating mirror streaking camera (RMC), it is necessary to make two adjustments, one in amplitude, the other in time. These adjustments are needed because the Fabry-Perot and the RMC are actually measuring two very different quantities. The RMC measures what might be called an "obscuration rate."

Referring to Fig. 3 for the geometry, the slit velocity can be written

$$V_S = V_d \tan\theta_S \qquad (5)$$

where V_S is the velocity as measured along the slit of the RMC, V_d is the detonation velocity of the HE, and θ_S is the local angle of the cylinder surface relative to the unperturbed surface. The Fabry-Perot measures the particle velocity scaled by the dot product of the particle direction and the laser beam direction. This can be written

$$V_{fp} = V_P \cos(\theta_P - \theta_L) \qquad (6)$$

where V_{fp} is the velocity as measured by the Fabry-Perot, V_P is the magnitude of the particle velocity, θ_P and θ_L are the angles formed by the particle trajectory and the laser with the original normal to the cylinder surface.

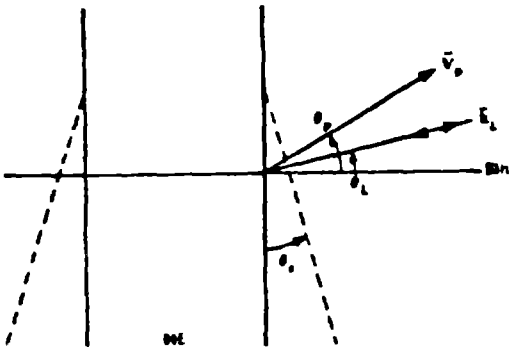

Fig. 3 Vector diagram of cylinder test wall motion.

θ_S and V_P are related through the hydrodynamics of the cylinder shot. Two simplifying assumptions make it possible to generate an analytical relation between them. First, that the flow is self similar, second that the particle trajectories are adequately approximated by straight lines. The second, assumption is supported by hydrodynamic code calculations. From these assumptions, a relation between V_S and V_{fp} can be generated of the form:

$$V_S(t) = AV_{fp}(t + \Delta t) \qquad (7)$$

where:

$$A = \left[\frac{\cos(\theta_P - \theta_L)}{\cos\theta_P} - V_{fp}(t + \Delta t)\frac{\tan\theta_P}{V_d}\right]^{-1},$$

$$\Delta t = r(t)\tan\theta_L/V_d,$$

and

$$r(t) = \int_0^t V_S(\tau)d\tau$$

This relation has been tested by using the HEMP code to calculate both the Fabry-Perot record and the record that would be seen by the RMC. The transform was identical to the hydrodynamic code results.

The procedure described above for converting Fabry-Perot velocity measurements to velocities in the RMC slit plane was used on the LX-14 experiments in which the radius/time history (Table 2) was measured with streak cameras. The average for the two experiments is presented in Fig. 4 and compared to the streak camera results in the next section.

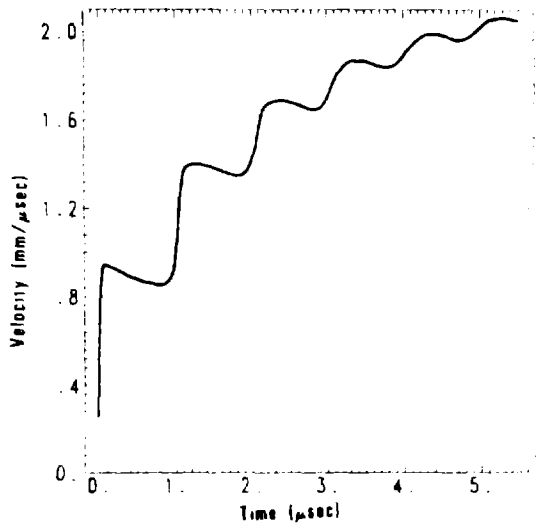

Fig. 4 Fabry-Perot determined average cylinder wall velocity from two LX-14 experiments.

Comparison of Fabry-Perot and RMC Results

Results from the different diagnostic techniques were compared in two ways, to examine reproducibility from experiment to experiment, and to examine any systematic difference between the diagnostic techniques. Table 3 compares wall velocities at $R - R_o = 6.5$ mm. Streak camera radius/time data has to be differentiated to make this comparison. Figure 5 presents the difference in expanded cylinder radius as a function of time. Fabry-Perot velocity/time data were integrated to make this comparison. The overall uncertainty in velocity is estimated as approximately 1/2% resulting in a 1% uncertainty in the cylinder wall energy.

TABLE 3
Cylinder Wall Velocity Comparison

Exp. No.	Density (gm/cc)	D (mm/μsec)	Average Velocity at $R-R_o$ = 6.5 mm	
			RMX	F-P
K520	1.830	8.79	1.986	1.980
K521	1.830	8.80	1.976	2.000

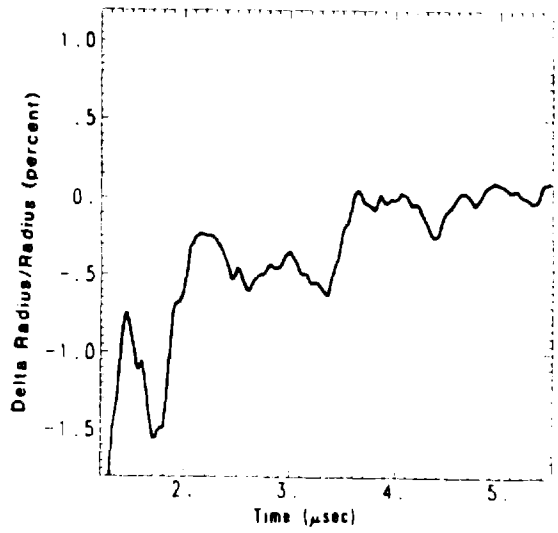

Fig. 5 Difference between streak cameras and Fabry-Perot velocimeters in cylinder radius/time history measurements for LX-14.

Hydrodynamic Calculations

LX-14 cylinder test calculations have been done using four different equations of state (EOS) for the detonation products. The CJ parameters and EOS constants are presented in Table 4. The JWL EOS 370A is based on earlier cylinder test data and an estimated P_{CJ} of 370 kbars. The JWL EOS 336A and the gamma law EOS 370G were used to illustrate the sensitivity of the calculated results to changes in EOS. The JWL EOS 360A is the revised EOS for LX-14 based on the experimental results presented in this paper.

TABLE 4
CJ Parameters and Equation of State Coefficients

Label	370A	360A	336A	370G	
Parameters					
P	.370	.360	.336	.370	mb
ρ	1.835	1.835	1.835	1.835	b/cm^{-3}
D	.880	.880	.883	.880	cm/ sec
E_o	.102	.102	.088	.1005	mb
Γ	2.84	2.947	3.258	2.84	
Coefficients					
A	8.261	11.65	129.46	-0-	
B	.1724	.5572	1.693	-0-	
C	.01296	.01844	.00183	.1303	
R_1	4.55	5.4	9.6	4.	
R_2	1.32	2.0	2.5	2.	
ω	.38	.45	.1	1.84	

Figure 6 presents cylinder wall velocities at early expansions calculated with equations of state having P_{CJ} of 370 kbars and P_{CJ} of 336 kbars. The results are almost identical showing that P_{CJ} does not uniquely determine early wall motion. The cylinder results, however, are sensitive to pressure and energy changes in an EOS at relative volumes for the detonation products greater than ~1.1. The flat plate test described below is used to resolve changes in an EOS at lower relative volumes.

The fractional energy change in the detonation products during expansion corresponds closely to the change in cylinder wall velocity squared. Figure 7 presents this detonation product energy change for various equations of state relative to that of JWL EOS 370A. Delta E is defined as:

$$\delta E = \frac{(\Delta E\ EOS(x) - \Delta E\ EOS\ 370A)}{\Delta E\ EOS\ 370A} \qquad (8)$$

The revised LX-14 EOS 360A is very close to EOS 370A at all expansions and they both match the experimental cylinder data within experimental error as shown in Fig. 8. (EOS 360A was chosen over that previously used because it is more consistent with the flat plate data described below.) EOS 336A matches cylinder results reasonably well at early expansions but underestimates cylinder wall velocities at larger expansions. The gamma law EOS 370G calculates wall velocities higher than experiment over the entire range of expansion.

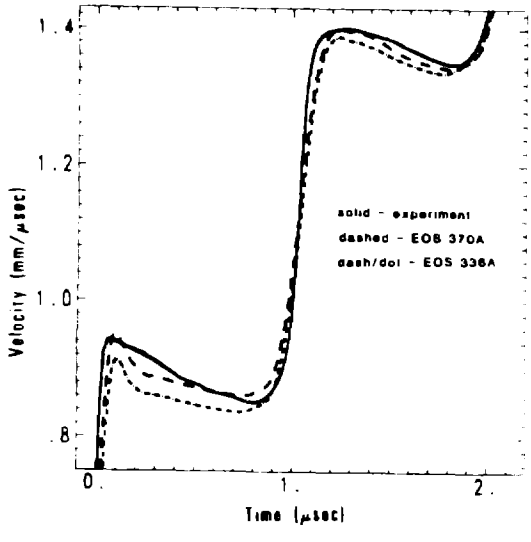

Fig. 6 Early cylinder motion calculated with P_{CJ} = 370 kbar and P_{CJ} = 336 kbar equations of state for LX-14.

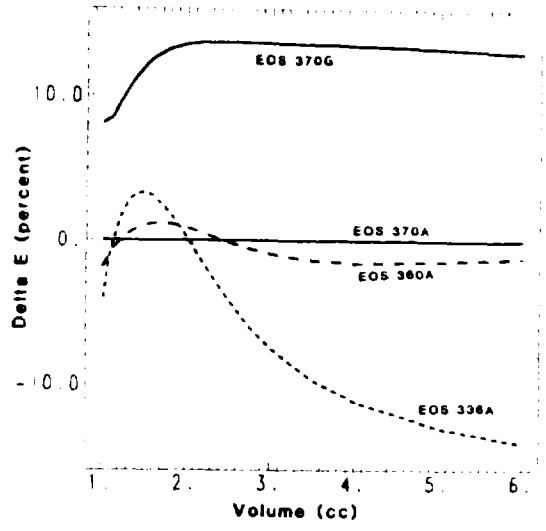

Fig. 7 The relative fractional energy change in the detonation products for the equations of state used in this study.

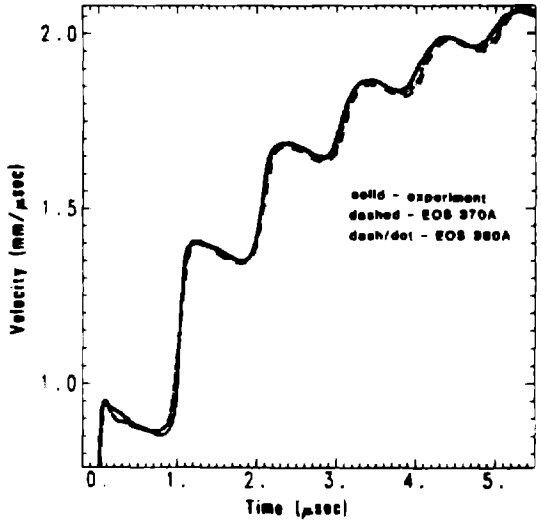

Fig. 8 Comparison of cylinder wall velocities predicted by the old and the revised equations of state with LX-14 experimental data.

FLAT PLATE TESTS

Experimental Results

Nineteen flat plate experiments using LX-14 and copper were performed in the geometries depicted in Fig. 2. They were grouped into five categories characterized by the ratio of the copper plate thickness to LX-14 thickness. See Table 5. These categories tend to emphasize different high pressure EOS regimes.

TABLE 5
Metal to Explosive Ratios for
Flat Plate Experiments

Length Cu/ Length LX-14	No. of Exps.	Plate Thickness (mm) Minimum	Maximum
0.001	3	0.025	0.025
0.006	5	0.123	0.257
0.013	1	0.126	0.126
0.026	9	0.505	2.502
0.053	1	0.532	0.532

The Fabry-Perot records for these experiments were reduced to velocity/time histories in a manner similar to that used in the cylinder test. However, a particle velocity vector correction was not necessary since the plate motion is aligned with the impinging laser light.

Detailed velocity/time histories similar to that shown in Fig. 9 were obtained for each experiment and were used in comparisons with hydrodynamic calculations. In order to summarize the results for this report, average velocities for various stages of plate acceleration were defined as shown in Fig. 9 and are presented in Table 6. Results for two LX-14 experiments with aluminum plates are also presented in Table 6.

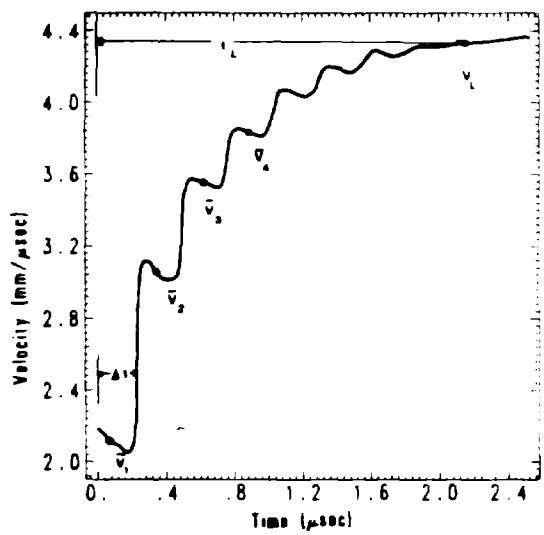

Fig. 9 Typical Fabry-Perot velocity results from the flat plate test. The average velocities and times depicted correspond to the to the values listed in Table 3.

Examination of the data presented in Table 6 shows significant scatter in early time velocities. Explosive inhomogenities due to the presence of large HMX crystals were considered a possible cause. However, the four experiments done with all fine grained HMX do not support this conclusion. Further work is required to pinpoint the cause of this scatter that is well outside the precision of the Fabry-Perot measurements.

Hydrodynamic Calculations

The detonation product equations of state listed in Table 3 and others were used to calculate the flat plate experiments. Figures 10 and 11 present the results from such calculations for a typical experiment. In the flat plate test the initial plate velocity is directly related to the detonation front pressure. As can be seen in Fig. 10, a gamma law EOS and a JWL EOS with P_{CJ} of 370 kbars give the same initial velocities. Subsequent velocity increments are substantially different, however. The gamma law EOS predicts velocities higher than measured, whereas the JWL EOS is in close agreement with this experiment.

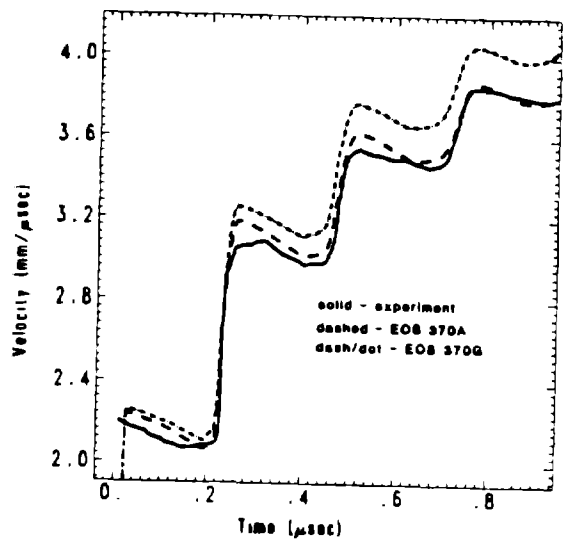

Fig. 10 Flat plate velocities predicted by two equations of state with P_{CJ} = 370 kbars.

Figure 11 presents results for two JWL equations of state with different detonation pressures. Similar comparisons for all the experiments in Table 6 lead to the choice of 360 kbars for P_{CJ} and the use of EOS 360A for the comparisons between calculations and experiments presented in the Table.

Table 6
Flat Plate Experiental Results

SHOT	#9642	#9643	#9632	#9495	#9579	#9526	#9635	#9636	#9524
Copper Thickness (mm)		.0254			.123	.126		.257	.126
LX-14 Length (mm)		25.58			20.18	19.97		40.15[c]	10.00
X_{Cu}/X_{LX-14}		.0010			.0061	.0063		.0064	.0126
$-\Delta t$[a] (μsec)		.01			.05	.05		.10	.05
$\bar{V}_1$ (mm/μsec)	2.43[b] (+10.5%)	2.49 (+13.5%)	2.63 (+19.5%)	2.10 (-2.5%)	-	2.20 (+2%)	2.24 (+3.5%)	2.05 (-5%)	2.11 (-2%)
$\bar{V}_2$ (mm/μsec)	3.56 (+5%)		3.66 (+7.5%)	3.16 (-5%)	3.17 (-4.5%)	3.22 (-3%)	3.36 (+1.0%)		
$\bar{V}_3$ (mm/μsec)	4.24 (+2.5%)	4.22 (+2.5%)	4.28 (+3.5%)	3.85 (-4%)	3.83 (-4.5%)	3.83 (-4.5%)	4.00 (0%)	3.88 (-3.5%)	3.72 (-3.5%)
$\bar{V}_4$ (mm/μsec)	4.68 (+1.5%)	4.64 (+.5%)							
$\bar{V}_L$ (mm/μsec)	5.60 (-1.5%)	5.48 (-.5%)					5.50 (+2%)	5.37 (-.5%)	
t_L (μsec)	.08	.076				1.0	1.0	1.0	1.0

SHOT	#BP1	#BP2	#9578	#9577	#9634	#9633	#9527	#BP5	#BP6	#9528
Copper Thickness (mm)	2.502	2.520	.505		.526		.530	2.530	2.530	.532
LX-14 Length (mm)	101.61	101.60	20.15		19.95[c]		20.00	92.02	91.07	10.01
X_{Cu}/X_{LX-14}	.0246	.0248	.0251		.0265		.0265	.0275	.0278	.0532
$-\Delta t$[a] (μsec)	1.00	1.00	.20		.20		.20	1.00	1.00	.20
$\bar{V}_1$ (mm/μsec)	2.14[b] (+1%)	2.17 (+2.5%)	2.02 (-4%)	2.22 (+6%)	2.12 (+1.5%)	2.12 (+1.5%)	2.11 (+1%)	2.11 (-.5%)	2.15 (+1.5%)	2.03 (+1%)
$\bar{V}_2$ (mm/μsec)	3.08 (+.5%)	3.16 (+3%)	3.04 (-1%)	3.09 (+1%)	3.07 (+1%)	3.03 (-.5%)	3.03 (-.5%)		3.06 (+.5%)	
$\bar{V}_3$ (mm/μsec)	3.60 (+1%)	3.67 (+3%)	3.62 (+2%)	3.60 (+1.5%)	3.55 (1%)	3.50 (-.5%)	3.57 (+1.5%)	3.55 (+.5%)	3.57 (+1%)	3.11 (+1.5%)
$\bar{V}_L$ (mm/μsec)			4.42 (+2%)		4.31 (+.5%)	4.35 (+1.5%)	4.35 (+2%)			
t_L (μsec)			2.0	2.0	2.0	2.0	2.0			1.4

Shot	#9586	#9587
Aluminum Thickness(mm)	.515	
LX-14 Length (mm)	20.23	
X_{Al}/X_{LX-14}	.0255	
$-\Delta t$[a] (μsec)	.17	
$\bar{V}_2$ (mm/μsec)	4.79 (+1.5%)	4.65 (-1.5%)
$\bar{V}_3$ (mm/μsec)	5.22 (+1.5%)	5.10 (-1%)
$\bar{V}_L$ (mm/μsec)	5.87 (+1%)	5.82 (0%)
t_L (μsec)	1.5	1.5

a See Fig. 9 for definition of t and V
b Numbers in ( ) are differences of experimental velocities and those calculated with LX-14 EOS #360A.
c Special formulation with small particle size HMX

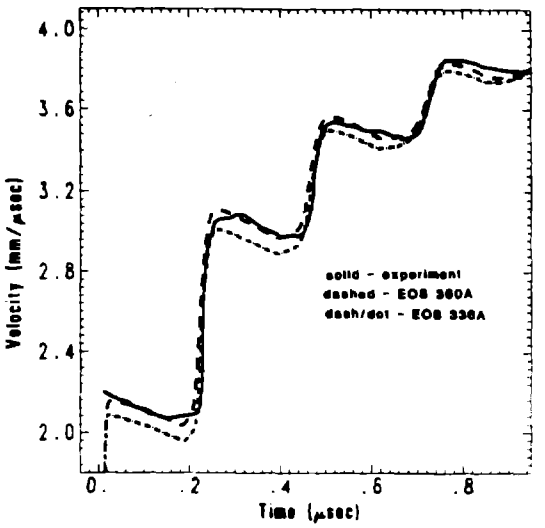

Fig. 11 Differences in flat plate velocities predicted by P_{CJ} = 360 kbar and P_{CJ} = 336 kbar equations of state.

The initial plate velocities measured for the very thin 0.025 mm copper plates are much higher than those measured for thicker plates. This clearly indicate that "von Neumann spike" effects are present. Figure 12 compares experiment to calculations done with and without a reactive flow model using the JWL 370A EOS for the products. The calculation using a reactive flow model proposed by Tarver[9] is in close agreement with the experiment.

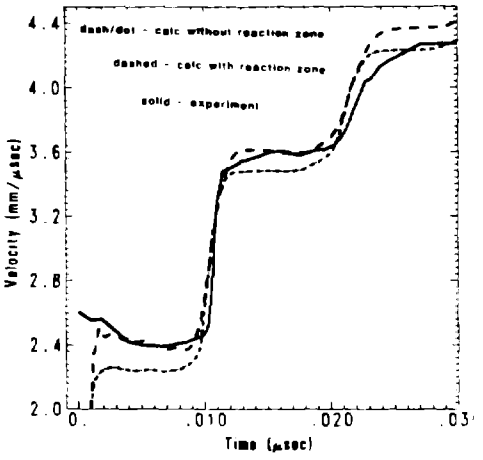

Fig. 12 Initial velocity of a very thin copper plate showed the effect of the reaction zone.

The comparisons of experiment with calculation presented in Table 6 show three regimes. For very thin plates (0.025 mm) the effect of the reaction zone is apparent. The measured early velocities are higher than those calculated without a reactive model. Experiments with plates about 0.1 to 0.2-mm thick have early velocities considerably less than those calculated. If the plate is thicker than about 0.5-mm, the calculations agree fairly closely with experiment. No single EOS could be found (even using the reactive model) which would bring the results from all three regimes into perfect agreement. This is strongly indicative of time-dependent effects taking place later than those normally associated with the LX-14 reaction zone. Investigations in this area are continuing.

Several calculations were run to show the effect of different equations of state on plate velocity for both a thin and thick copper plate accelerated by 30-mm of LX-14. Figure 13 shows the pressure difference for the two equations of state, EOS 370A and EOS 336A, where:

$$\delta P = [P\ EOS\ 336A] - [P\ EOS\ 370A] \qquad (9)$$

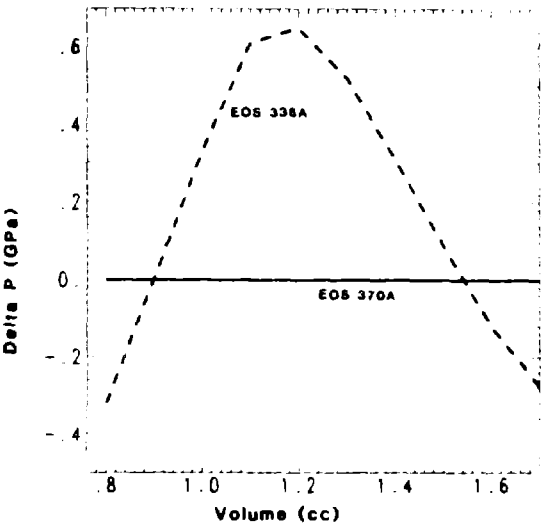

Fig. 13 Differences in pressure at small relative volumes for P_{CJ} = 370 kbar and P_{CJ} = 336 kbar equations of state.

Figure 14 presents the results for the 0.127-mm copper plate. The initial velocity difference is due to the difference in P_{CJ}. The later velocities are primarily determined by the differences in pressure below a relative volume of 1.1.

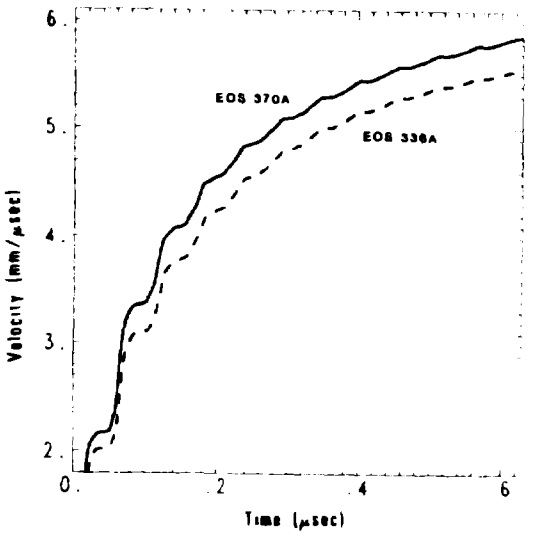

Fig. 14 Differences in "thin" plate velocities predicted by P_{CJ} = 370 kbar and P_{CJ} 336 kbar equations of state.

Figure 15 presents the calculations for the 0.635-mm plate. This plate is five times as thick as the "thin" plate discussed above. The initial velocity difference is again determined by the differences in P_{CJ}. The velocity difference at later times however decreases because in this case the velocity history is determined by the pressure at relative volume up to about 1.5.

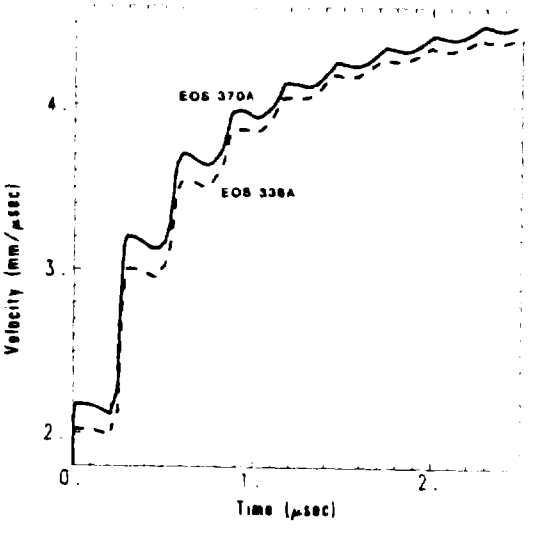

Fig. 15 Differences in "thick" plate velocities predicted by P_{CJ} = 370 kbar and P_{CJ} = 336 kbar equations of state.

CONCLUSIONS

Improvements have been made in experimental procedures and analysis and hydrodynamic calculations which permit a more precise determination of the equation of state of explosives. Experiments measuring the early expansion data of the products of LX-14 were reproducible to within 4% in energy while those emphasizing larger expansions were within 2% in energy. The empirical detonation product equation of state thus generated is useful both for designing metal/explosive assemblies and as a check on "first principle" equations of state.

The conventional definition of P_{CJ} was used throughout as a convenient initial condition at the shock front. We have considered "von Neumann spike" phenomena and accounted for the effects. We have not treated the problem of kinetic effects with longer time scales but have certainly not ruled out such effects. An "effective" shock front pressure and particle velocity corresponding to P_{CJ} = 360 kbars are consistent with the experimental results described here.

If the products are treated as an equilibrium mixture of gases and condensed phases, the expansion described here is the proper description. On this basis our results show that the isentrope index $\Gamma = (\partial \ln P/\partial \ln V)_S$ must increase for increasing volume in the region of $V_{CJ} < V < 1.1$ in order to match the experimental data.

There is a small but clearly discernible discrepancy between the "thin" plate and "thick" plate results which has not been resolved by varying the EOS. Further experimental tests will be required to establish the exact nature of this discrepancy. Nevertheless kinetic effects beyond the "von Neumann spike" must be considered.

We believe that a consistent treatment of longer time scale (>0.1 μs) kinetic effects such as the formation of solid carbon following the detonation front may very well be required to explain the experimental results and would alter this equilibrium description.

ACKNOWLEDGMENT

We wish to acknowledge the considerable contributions of C. Pruneda, L. Meegan, and H. Chau to material preparation, test assembly and Fabry-Perot operation.

REFERENCES

1. H. Jones and A. R. Miller, "The Detonation of Solid Explosives," Proc. Roy. Soc. London, A-194, 480 (1948).

2. J. M. Walsh, M. H. Rice, R. G. McQueen, and F. L. Yarger, "Shock-Wave Compressions of Twenty-Seven Metals. Equations of State of Metals," Phys. Rev. 108, 196-216 (1957).

3. W. E. Deal, "Measurement of the Reflected Shock Hugoniot and Isentrope for Explosive Reaction Products," J. Chem. Phys. 27, 796 (1957).

4. E. L. Lee, H. C. Hornig, J. W. Kury, "Adiabatic Expansion of High Explosive Detonation Products," UCRL-50422, TID-4500, UC-4 Chemistry, Lawrence Radiation Laboratory, University of California, Livermore, CA, May 2, 1968.

5. H. Chau, D. Goosman, J. Lyle, and M. Summers, "A Simple Velocity Interferometer System," Conference on Laser and Electro-optical Systems, OSA/IEEE, Abstract TUHH4, p. 20 (1978).

6. M. L. Wilkins, "Methods in Computational Physics, " Vol. 3 Academic Press Inc., N.Y., 1964, pp. 211-263.

7. R. C. Weingart, et. al., "Acceleration of Thin Flyers by Exploding Metal Foils: Application to Initiation Studies," Sixth Symposium (International) on Detonation, August 1976.

8. J. P. Woodruff, "KOVEC User's Manual," Lawrence Livermore National Laboratory Report, UCID-17306, September 1976.

9. C. M. Tarver, et. al., "Modeling Short Pulse Duration Shock Initiation of Solid Explosives," Eighth Symposium (International) on Detonation, July 1985.